Volume 38
Number 10
October 2023
Pages 1897–2204

JAAS

Journal of Analytical Atomic Spectrometry

rsc.li/jaas

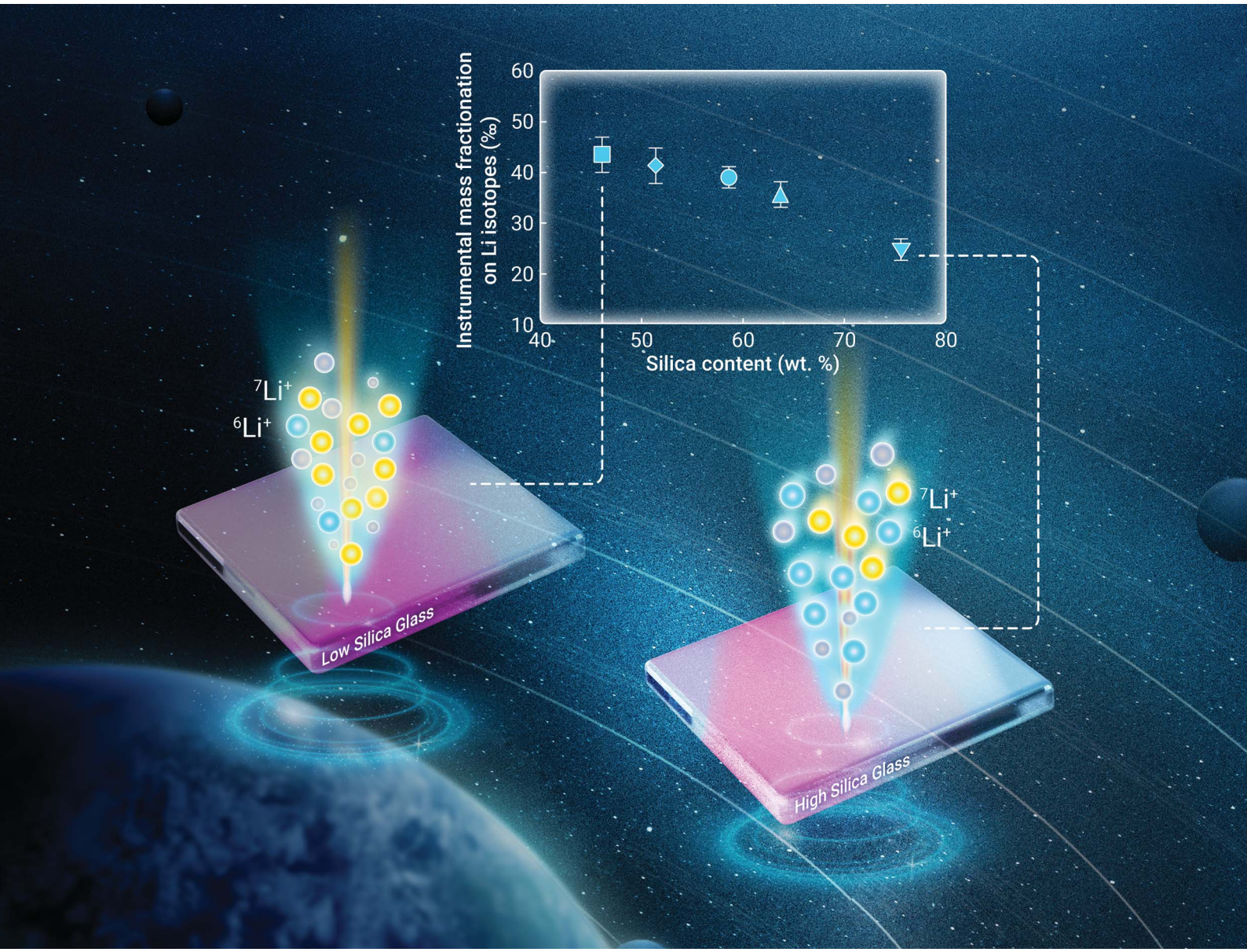

ISSN 0267-9477

ROYAL SOCIETY OF CHEMISTRY

PAPER

Wei Yang *et al.*

A silica-related matrix effect on NanoSIMS Li isotopic analysis of glasses and its online calibration

JAAS

PAPER

View Article Online
View Journal | View Issue

Open Access Article. Published on 30 August 2023. Downloaded on 1/27/2026 4:47:07 AM.
This article is licensed under a Creative Commons Attribution-NonCommercial 3.0 Unported Licence.

Check for updates

Cite this: *J. Anal. At. Spectrom.*, 2023, **38**, 1962

A silica-related matrix effect on NanoSIMS Li isotopic analysis of glasses and its online calibration

Rui-Ying Li, Jialong Hao, Wei Yang,* Heng-Ci Tian, Sen Hu and Yangting Lin

Accurate Li isotope analysis of silicate glasses using secondary ion mass spectrometry (SIMS) is challenging due to the matrix effect, which causes instrumental mass fractionation (IMF). The characteristics of the matrix effect vary for each element, necessitating empirical correction methods. Here, we present Li isotopic measurements on a set of silicate glasses spanning a broad compositional range from ultramafic to highly siliceous using a Cameca NanoSIMS 50L. A radio-frequency (RF)-O primary beam with an intensity of 1 nA was rastered over a 5 × 5 μm^2 area on the sample, and the secondary ions ^{6}Li, ^{7}Li and ^{30}Si were simultaneously detected. We observed a significant matrix effect on δ^7Li in the silicate glasses, which yielded an IMF of up to 19‰, exceeding the analytical precision of <2.5‰ (1SD). The IMF is strongly correlated with the chemical compositions of the silicate glasses. To correct the matrix effect, we employed various correction schemes, including univariate and multivariable compositions. All results consistently indicated that silica exerted a dominant influence on the IMF. We then propose a straightforward "online" method to correct this silica-related matrix effect by utilizing simultaneously measured ^{30}Si signals. This strategy improves the accuracy of the Li isotope measurements to within 3‰ and can be widely applied to anhydrous subalkaline magmatic glasses with compositions ranging from ultramafic to highly siliceous.

Received 24th March 2023
Accepted 17th August 2023

DOI: 10.1039/d3ja00100h

rsc.li/jaas

1. Introduction

Lithium is the lightest metal element with two stable isotopes – ^{6}Li (7.52%) and ^{7}Li (92.48%). The large mass difference (16%) between its isotopes results in considerable variations of Li isotopes in geological processes, making Li isotopes a geochemical tracer with broad applications. Due to the strong fluid mobility of Li, its isotopes are powerful tracers for the processes of mantle convection and crust/mantle recycling,[1–4] as well as planetary weathering.[5–9] Owing to the rapid diffusivity of Li and associated isotopic fractionations on meter-to-micrometer scales, Li isotopes have been employed as high-resolution geo-speedometers to reveal the history of magmatic exhalation[10–14] and fluid–rock interactions.[15] In addition, Li has also provided valuable information regarding Big Bang nucleosynthesis and the subsequent cosmic and stellar evolution.[16–23]

The secondary ion mass spectrometry (SIMS) technique is widely used for Li isotope measurements and offers the advantage of efficiently assessing spatial correlations between concentration and isotopes at the micrometer scale.[4,10,12,16–18,24–32] However, SIMS analysis is significantly affected by the matrix effect, leading to instrumental mass fractionation (IMF) that is critically dependent on the chemical compositions and/or structure of the analyte.[4,24–26,28–31,33–43] Moreover, the characteristics of the matrix effect generally differ depending on the element, making the correction complex. In the case of Li measurement, previous studies have observed composition-dependent bias in minerals and silicate glasses.[24–26,29–31,39] For Li concentration analysis, a Si-related matrix effect on silicates[25,29] and an (Fe + Mn)-related matrix effect on tourmaline[30] have been noted. Regarding Li isotope analysis, a Mg/(Mg + Fe)-related matrix effect on olivine[24,31] and an (Fe + Mn)-related matrix effect on garnet[39] were reported. Although SIMS energy filtering can be used to reduce the matrix effect, it could result in a signal loss for the desired secondary ions and unwanted effects for other simultaneously measured elements.[26,29] A commonly used method to correct the matrix effect is to calibrate the unknown samples against matrix-matched reference materials with known concentrations and isotopic compositions.[24,25,31,33,34,36–41,44–47] However, the reference materials may not always match the unknowns in composition. Therefore, it is necessary to develop a calibration strategy for the matrix effect on Li isotope analysis that can be applied to a wide range of samples.

This study aims to quantify the matrix effect on Li isotope analysis of silicate glasses and establish correction schemes applicable to glasses with a compositional range from komatiite to rhyolite. A NanoSIMS was used due to its high spatial

Key Laboratory of Earth and Planetary Physics, Institute of Geology and Geophysics, Chinese Academy of Sciences, Beijing 100029, P. R. China. E-mail: yangw@mail.iggcas.ac.cn

 This journal is © The Royal Society of Chemistry 2023

Open Access Article. Published on 30 August 2023. Downloaded on 1/27/2026 4:47:07 AM.
This article is licensed under a Creative Commons Attribution-NonCommercial 3.0 Unported Licence.

resolution and multi-collection mode to measure Li isotopes with other elements.[32,35,36,40,41,43,47–58]

2. Samples and analytical procedures

2.1 Sample preparation

Five MPI-DING glasses spanning a wide range from ultramafic to highly siliceous composition were chosen for analysis, including GOR128-G (komatiite), ML3B-G (basalt), StHs6/80-G (andesite), T1-G (diorite) and ATHO-G (rhyolite). These samples were prepared by fusing natural rock powders.[59] Detailed chemical compositions of these MPI-DING samples have been published by Jochum (2006).[60] Preferred values for Li concentrations and Li isotopes are in range of 4.5–28.6 ppm and 2.1–17.1‰, respectively.[60] Their compositions are summarized in Table 1. Fragments of the standard samples were cast in a tin–bismuth alloy mount and well-polished to expose the interior of the crystals. The sample mount was washed by ultrasonic cleaning in ethanol and coated with high-purity gold prior to analysis.

2.2 Analytical conditions

We performed Li analyses using the Cameca NanoSIMS 50L instrument at the Institute of Geology and Geophysics, Chinese Academy of Sciences (IGGCAS) in Beijing. A radio-frequency (RF)-plasma source was applied to generate an $^{16}O^-$ primary beam with an impact energy of 16 keV and an intensity of 1 nA. A mass resolution ($M/\Delta M$ measured at a 10% peak height) of ~5000 was set to separate any possible interference (*e.g.*, $^6LiH^+$) from the peaks of interest. Positive ^6Li, ^7Li and ^{30}Si ions were simultaneously detected using electron multipliers (EMs) with 44 ns dead-time correction. Each analytical spot was pre-sputtering by 10 × 10 μm^2 for ~60 s to remove the coating and implant $^{16}O^-$ into the samples to stabilize the yield of the secondary ions. Afterward, the secondary ions were acquired from the central raster of 5 × 5 μm^2. Each analysis consisted of 50 blocks of 20 cycles, with 64 × 64 pixels for a single cycle and a default counting time of 132 μs for each pixel. Then, the analytical sequences were set in the chained analysis mode of the NanoSIMS for the standard samples. The secondary ion beam centering at the entrance silt proceeded automatically after the pre-sputter. The total analysis time was approximately 10–11 min with a counting time of 9 min. The whole experiment was conducted in 3 sessions over three days, with each standard sample measured 25 times repeatedly. To eliminate the impact of potential sensitivity degradation of EMs, each EM was monitored and corrected using the pulse height distribution (PHD) curve every 12 hours.

Then, the Li isotope and IMF values were expressed in per mil deviations as follows:

$$\delta^7Li_{measured} = [(^7Li/^6Li_{measured})/(^7Li/^6Li_{\ L\text{-}SVEC}) - 1] \times 1000 \quad (1)$$

$$IMF = [(^7Li/^6Li_{measured})/(^7Li/^6Li_{true}) - 1)] \times 1000 \quad (2)$$

$$\delta^7Li_{calibrated} = \delta^7Li_{measured} - IMF \quad (3)$$

where L-SVEC is the international carbonate standard for Li isotopes with a recommended $^7Li/^6Li$ ratio of 12.0192;[36] $^7Li/^6Li_{true}$ and $^7Li/^6Li_{measured}$ are the NanoSIMS reference value (Table 1) and measured value (Table 2) of the glass standards, respectively.

Table 1 Summary of preferred compositions for glass standards used in this study

	GOR128-G	ML3B-G	T1-G	StHs6/80-G	ATHO-G
Compositions	Komatiite	Basalt	Diorite	Andesite	Rhyolite
SiO_2[a] (wt%)	46.1 ± 0.4	51.4 ± 0.6	58.6 ± 0.4	63.7 ± 0.5	75.6 ± 0.7
MgO[a] (wt%)	26.00 ± 0.30	6.59 ± 0.08	3.75 ± 0.04	1.97 ± 0.04	0.103 ± 0.01
Al_2O_3[a] (wt%)	9.9 ± 0.2	13.6 ± 0.2	17.1 ± 0.2	17.8 ± 0.2	12.2 ± 0.2
FeO_t[a] (wt%)	9.81 ± 0.12	10.90 ± 0.10	6.44 ± 0.06	4.37 ± 0.07	3.27 ± 0.10
CaO[a] (wt%)	6.2 ± 0.1	10.5 ± 0.1	7.1 ± 0.09	5.3 ± 0.1	1.7 ± 0.03
TiO_2[a] (wt%)	0.29 ± 0.01	2.13 ± 0.09	0.76 ± 0.02	0.70 ± 0.02	0.26 ± 0.02
K_2O[a] (wt%)	0.04 ± 0.01	0.39 ± 0.09	1.96 ± 0.02	1.29 ± 0.02	2.64 ± 0.02
Na_2O[a] (wt%)	0.57 ± 0.03	2.40 ± 0.06	3.13 ± 0.09	4.44 ± 0.14	3.75 ± 0.31
P_2O_5[a] (wt%)	0.03 ± 0.01	0.23 ± 0.023	0.17 ± 0.03	0.16 ± 0.02	0.03 ± 0.004
MnO[a] (wt%)	0.18 ± 0.01	0.17 ± 0.01	0.13 ± 0.01	0.08 ± 0.004	0.11 ± 0.01
$K_2O + Na_2O$ (wt%)	0.61	2.79	5.09	5.73	6.39
H_2O[a] (wt%)	0.026	0.015	0.026	0.025	0.014
CO_2[a] (ppm)	4.4	4.7	6.3	4.4	3.7
Li[a] (ppm)	10.4 ± 1.7	4.5 ± 0.4	19.9 ± 0.9	20.7 ± 2.3	28.6 ± 1.8
$^7Li/^6Li_{true}$	12.0336	12.0236	12.0213	12.0228	12.0363
δ^7Li[a] (‰)	14.4 ± 0.4	4.4 ± 0.4	2.1 ± 0.4	3.6 ± 0.4	17.1 ± 0.4
NBO/T[b]	1.88	0.84	0.38	0.19	0.07
MAM[c]	22.0	22.9	22.2	21.6	21.5

[a] The chemical and Li isotopic compositions with uncertainties (1SD) of the glass standards are from Jochum (2006).[60] Li isotopes are given relative to the reference material L-SVEC. [b] NBO/T: the ratio of non-bridging oxygen atoms per tetrahedrally coordinated cations, calculated as NBO/T = 2 $(X_{MgO} + X_{CaO} + X_{FeO} + X_{MnO} + X_{Na_2O} + X_{K_2O} - X_{Al_2O_3})/(X_{SiO_2} + 2X_{Al_2O_3})$ following the reference,[61] and X is the mole fraction of the corresponding elements. [c] MAM: the mean atomic mass.

Open Access Article. Published on 30 August 2023. Downloaded on 1/27/2026 4:47:07 AM.
This article is licensed under a Creative Commons Attribution-NonCommercial 3.0 Unported Licence.

Table 2 Data summary of Li analysis for silicate glasses in sessions 1, 2 and 3

Analytical sessions	Samples	^{7}Li rate (cps)	RSD[a] (%)	^{30}Si rate (cps)	RSD[a] (%)	^{7}Li/^{6}Li$_{measured}$	δ^{7}Li$_{measured}$ (‰)	SD[b] (‰)	IMF (‰)	n
Session 1	ATHO-G	2.96×10^4	1.03	4.36×10^5	0.89	12.5279	42.3	1.2	24.8	5
	GOR128-G	1.14×10^4	1.61	1.72×10^5	0.83	12.7226	58.5	1.9	43.5	5
	StHs6/80-G	2.38×10^4	0.80	2.93×10^5	0.35	12.4925	39.4	1.4	35.7	5
	T1-G	2.48×10^4	0.40	2.49×10^5	1.09	12.5147	41.2	1.2	39.0	5
	ML3B-G	5.76×10^3	0.41	2.03×10^5	0.47	12.5711	45.9	1.9	41.3	5
Session 2	ATHO-G	2.65×10^4	1.89	4.15×10^5	0.87	12.6163	49.7	2.3	32.0	10
	GOR128-G	1.09×10^4	2.58	1.66×10^5	1.37	12.7577	61.4	1.7	46.4	10
	StHs6/80-G	2.28×10^4	0.77	2.85×10^5	0.61	12.4675	37.3	2.3	33.3	10
	T1-G	2.41×10^4	1.33	2.44×10^5	0.78	12.5149	41.2	1.9	39.1	10
	ML3B-G	5.27×10^3	1.45	1.94×10^5	0.54	12.6098	49.1	2.5	44.5	10
Session 3	ATHO-G	2.98×10^4	1.40	4.35×10^5	0.63	12.4690	37.4	1.8	20.0	10
	GOR128-G	1.06×10^4	4.26	1.64×10^5	1.58	12.6305	50.9	2.3	35.9	10
	StHs6/80-G	2.46×10^4	1.06	2.92×10^5	0.69	12.3844	30.4	1.4	26.7	10
	T1-G	2.51×10^4	2.35	2.45×10^5	0.89	12.4722	37.7	1.9	35.5	10
	ML3B-G	5.66×10^3	1.82	1.96×10^5	0.74	12.5294	42.5	2.1	37.9	10

[a] RSD represents the relative standard deviation of ^{7}Li and ^{30}Si counting rates for repeated analysis of samples in a single session. [b] SD represents the standard deviation of δ^{7}Li$_{measured}$ values for repeated analysis of samples in a single session.

3. Results

3.1 Li yields and IMF

ATHO-G, with the highest Li concentration of 28.6 ± 1.8 ppm among these samples (Table 1), shows a ^{7}Li counting rate ranging from 2.65×10^4 to 2.98×10^4 counts per second (cps) in three analytical sessions (Table 2). For each session, the relative standard deviation (RSD) of its ^{7}Li counting rate ranges between 1.03% and 1.89% (Table 2). The average ^{7}Li^{+} yield of ATHO-G can be calculated to be approximately 1001 ± 65 cps nA^{-1} ppm^{-1}. The measured δ^{7}Li value of ATHO-G varies from 37.4‰ to 49.7‰ in the three sessions (Table 2). Accordingly, the IMF of ATHO-G ranges from 20.0‰ to 32.0‰ (Table 2).

StHs6/80-G has a Li abundance of 20.7 ± 2.3 ppm (Table 1). It gains a ^{7}Li counting rate of 2.28×10^4–2.46×10^4 cps with RSD values of 0.77–1.06% (Table 2) and a ^{7}Li^{+} yield of 1147 ± 43 cps nA^{-1} ppm^{-1}. The measured δ^{7}Li value is 30.4–39.4‰, with the IMF calculated to be 26.7–35.7‰ (Table 2).

The Li concentration of T1-G is 19.9 ± 0.9 ppm (Table 1). T1-G yields ^{7}Li counting rates of 2.41×10^4–2.51×10^4 with RSD values of 0.40–2.35% (Table 2). The average yield of ^{7}Li^{+} is 1239 ± 24 cps nA^{-1} ppm^{-1} for T1-G. The measured δ^{7}Li value is 37.7–41.2‰ (Table 2). As a result, the IMF is calculated to be 35.5–39.1‰ (Table 2).

GOR128-G has 10.4 ± 1.7 ppm Li (Table 1), and a range of ^{7}Li counting rates of 1.06×10^4–1.14×10^4 (Table 2). The relative

Table 3 Summary of parameters in Li *in situ* analysis from previous studies

Instruments	Analytical model	Primary beam intensity (nA)	Raster size (μm)	Precision (‰)	Ref.
NanoSIMS	Multi-collection	1	5	1.2–2.5[a]	This study
SIMS	Multi-collection	15	20	1[a]	4
SIMS	Magnetic peak switching	30	30	1.5[b]	12
SIMS	Magnetic peak switching	40	30	0.6[a]	13
SIMS	Magnetic peak switching	50	25	0.5–2.8[a]	17
SIMS	Magnetic peak switching	10	5[c]	1–2[a]	18
SIMS	Magnetic peak switching	15–30	30–50	0.7–1[a]	24
SIMS	Magnetic peak switching	20	25	0.2–1[a]	26
SIMS	Multi-collection	3–17	20	0.3–1.8[b]	39
SIMS	Magnetic peak switching	20	12	0.5–1[a]	62
SIMS	Magnetic peak switching	10–20	25	2[a]	63
SIMS	Magnetic peak switching	14–30	5–20	2–5[a]	64
LA-MC-ICPMS	Multi-collection	n. d.	125–150	0.5[a]	65
SIMS	Magnetic peak switching	14–30	20–30	1[a]	66
LA-MC-ICPMS	Multi-collection	n. d.	65–120	<1[a]	67
SIMS	Magnetic peak switching	28	20–30	1[a]	68
SIMS	Magnetic peak switching	1–5	10–20	0.5–2.5[a]	69
LA-MC-ICPMS	Multi-collection	n. d.	26	1[a]	70

[a] The precision is reported as 1SD for δ^{7}Li. [b] The precision is reported as 1SE for δ^{7}Li. [c] The beam size of the corresponding primary beam. The raster size in other studies represents the size of analytical area.

 This journal is © The Royal Society of Chemistry 2023

Open Access Article. Published on 30 August 2023. Downloaded on 1/27/2026 4:47:07 AM.
This article is licensed under a Creative Commons Attribution-NonCommercial 3.0 Unported Licence.

variation of ^{7}Li counting rates for GOR128-G is 1.61–4.26%, which is higher than that of other samples in each session (Table 2). Its average yield of $^{7}Li^{+}$ is calculated to be 1055 ± 41 cps nA^{-1} ppm^{-1}. The measured δ^{7}Li value of GOR128-G is 50.9–61.4‰ with an IMF of 35.9–46.4‰ (Table 2).

ML3B-G has the lowest Li abundance of 4.5 ± 0.4 ppm in this study (Table 1). It gains ^{7}Li counting rates of 5.27 × 10^{3}–5.76 × 10^{3} cps with RSD values of 0.41–1.82% (Table 2). The yield of $^{7}Li^{+}$ for ML3B-G is 1236 ± 58 cpsn A^{-1} ppm^{-1}. And the measured δ^{7}Li value is 42.4–49.1‰, with the IMF varying from 37.9‰ to 44.5‰ (Table 2).

In summary, the ^{7}Li counting rate is correlated with the Li abundance of the sample, while the RSD values of the counting rate mirror the instrumental steady-state and the uncertainty of the samples. The yield of Li ions and IMF values vary from sample to sample. The difference in IMF among various types of silicate glasses could reach 19‰ in a single session, resulting from the matrix effect on Li isotope analysis of silicate glasses (Table 2). A systematic ^{7}Li/^{6}Li ratio variation was observed for the same samples in different analytical sessions (Table 2). Comparisons of these sessions show variable IMF for a given sample (up to 12‰, Table 2), suggesting that the IMF is quite sensitive to slight shifts in the instrumental conditions.

3.2 Analytical precision

The analytical precision of the ^{7}Li/^{6}Li ratio determination is evaluated in terms of internal (within-spot analysis, SE) and external (spot-to-spot analysis, SD) precision. The internal precision of the ^{7}Li/^{6}Li ratio for each analytical point ranges from 0.9‰ to 2.1‰ (1SE), following the Poisson theoretical error determined qualitatively from counting statistics of ^{7}Li and ^{6}Li. Typically, it decreases with increasing Li concentration in the analyzed phase. The external precision of ^{7}Li/^{6}Li ratios over repeated analysis ranges from 1.2‰ to 2.5‰ (1SD) in a single analytical session (Table 2).

Previous *in situ* Li isotope analytical methods established by SIMS and laser ablation-multiple collector-inductively coupled plasma-mass spectrometry (LA-MC-ICP-MS) have yielded a general reproducibility within 1–3‰ (1SD) (Table 3). Given the low abundance of Li in most of the samples, primary beam intensities with tens of nA were applied in the raster sizes of tens to hundreds of micrometers (Table 3). It is notable that the spatial resolution of Li isotope measurements in this study is ~5 μm, significantly better than that in previous studies with comparable analytical reproducibility.

4. Discussion

The results from this study show that the relative IMF among silicate glasses can differ by up to 19‰ in a single session, far beyond the current analytical precision of <2.5‰ (1SD) (Table 2). These data presented by silicate glasses offer productive examples to investigate the matrix effect caused by variable chemical composition. Here, we evaluate several composition-dependent correction schemes for calibrating the IMF of Li isotope analysis in silicate glasses.

4.1 Effects of non-bridging oxygen on IMF

Li ions in silicate glasses are coordinated with non-bridging oxygen (NBO). Studies on alkali-silicate glasses proposed that the insertion of Li and other alkali cations increases NBO sites and influences the glass properties (*e.g.*, electrical conductivity).[71–74] Thus, it is necessary to explore the effect of NBO on Li isotope-IMF variation. We estimated NBO/T following the method of Seetharaman (2013),[61] with Na, K, Ca, Fe, Mg and Mn assumed to be network modifiers (NBO) and Si and Al to be network formers (T) (Table 1). The positive correlations between NBO/T and IMF are observed (Fig. 1). A best-fit empirical equation in the logarithmic form of IMF = a × ln(NBO/T) + c could be gained, with regression coefficient (R^2) values ranging from 0.81 to 0.94 for different sessions (Fig. 1). Using the logarithmic fit as a correction scheme, 73% of the δ^{7}Li values are reproduced within ±3‰ of their reference values. Such observations suggest that the IMF correction scheme based on NBO/T could be useful. However, the NBO/T values are estimated using the chemical compositions of the silicate

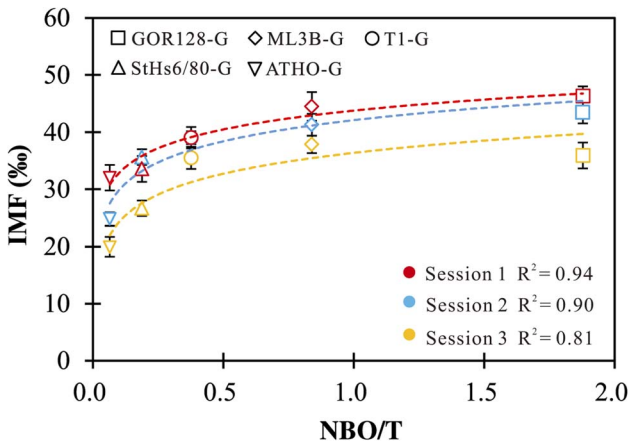

Fig. 1 IMF values as a function of NBO/T of silicate glasses. The vertical error bars are the external precision of the measurements.

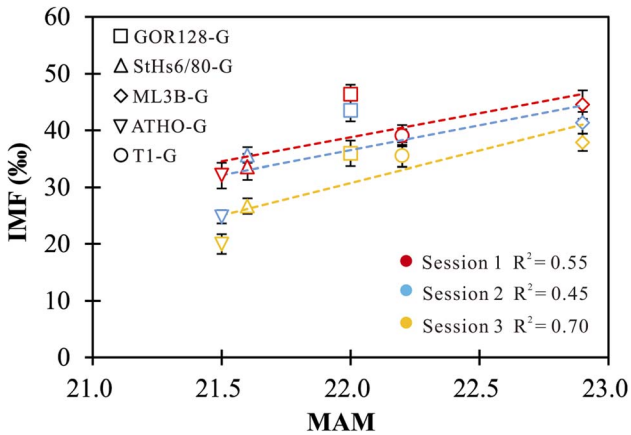

Fig. 2 The correlations between IMF and MAM of silicate glasses. The vertical error bars represent the external precision of the measurements.

Open Access Article. Published on 30 August 2023. Downloaded on 1/27/2026 4:47:07 AM.
This article is licensed under a Creative Commons Attribution-NonCommercial 3.0 Unported Licence.

glasses. In other words, different chemistry induces variation in the properties of silicate glasses, which in turn have an impact on the IMF of Li.

4.2 Effects of mean atomic mass on IMF

The effect of mean atomic mass (MAM) on IMF has been previously proposed in the investigations of O isotopes of samples.[33,34,37,38,42] Eiler *et al.* (1997)[34] and Hervig *et al.* (1992)[38] revealed considerable correlations between the O-isotope IMF and the MAM for both minerals and silicate glasses, while no robust connection was observed in other studies.[33,37,42] In this study, positive correlations between the Li-isotope IMF and the MAM of the investigated silicate glasses are observed, but they are not sufficiently robust (Fig. 2). The MAM is an integrated parameter that fundamentally depends on compositions. The correlations between the MAM and IMF cannot isolate the influence caused by the changes in chemical compositions. In this regard, using an IMF-correction scheme based on the MAM does not offer a significant advantage.

4.3 Effects of chemical compositions on IMF

The chemical compositions of the investigated silicate glasses vary from ultramafic to highly siliceous covering a broad range of compositions. Both single and combined component effects on IMF variations are considered below.

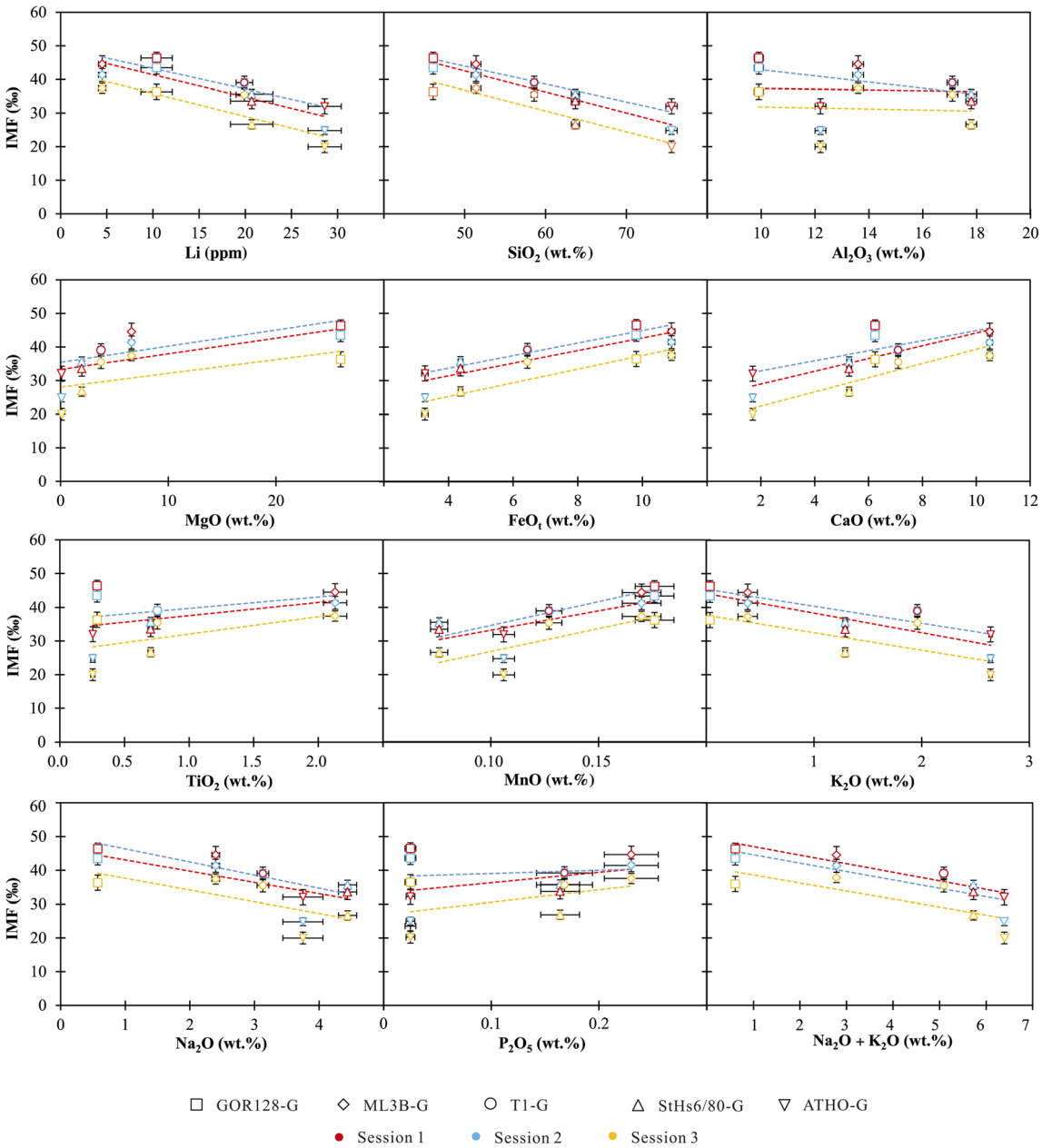

Fig. 3 IMF as a function of single chemical compositions in silicate glasses. The vertical bars are the external precisions of the measurements, and the horizontal bars represent the precisions of the reference values from Jochum *et al.* (2006).[60]

Open Access Article. Published on 30 August 2023. Downloaded on 1/27/2026 4:47:07 AM.
This article is licensed under a Creative Commons Attribution-NonCommercial 3.0 Unported Licence.

4.3.1 Univariate correction schemes. For the single chemical compositions, we observed that the IMF values are negatively correlated with the SiO_2, K_2O, and Na_2O contents and Li concentration, and positively correlated with MgO, FeO_t, CaO and MnO contents (Fig. 3). There are no apparent correlations between IMF and Al_2O_3, TiO_2 and P_2O_5 contents (Fig. 3). If taken total alkalis contents into account, the correlations performed

Table 4 The R^2 values for the best-fit linear regression lines calculated for various correlations between IMF with univariable composition of the silicate glasses

R^2 for sessions	Li	SiO_2	Al_2O_3	MgO	FeO_t	CaO	TiO_2	MnO	K_2O	Na_2O	P_2O_5	$K_2O + Na_2O$
Session 1	0.74	0.95	0.01	0.45	0.72	0.68	0.17	0.45	0.74	0.45	0.15	0.90
Session 2	0.82	0.91	0.23	0.63	0.95	0.56	0.16	0.89	0.73	0.81	0.02	0.65
Session 3	0.74	0.87	0.01	0.32	0.80	0.79	0.27	0.59	0.55	0.46	0.21	0.55

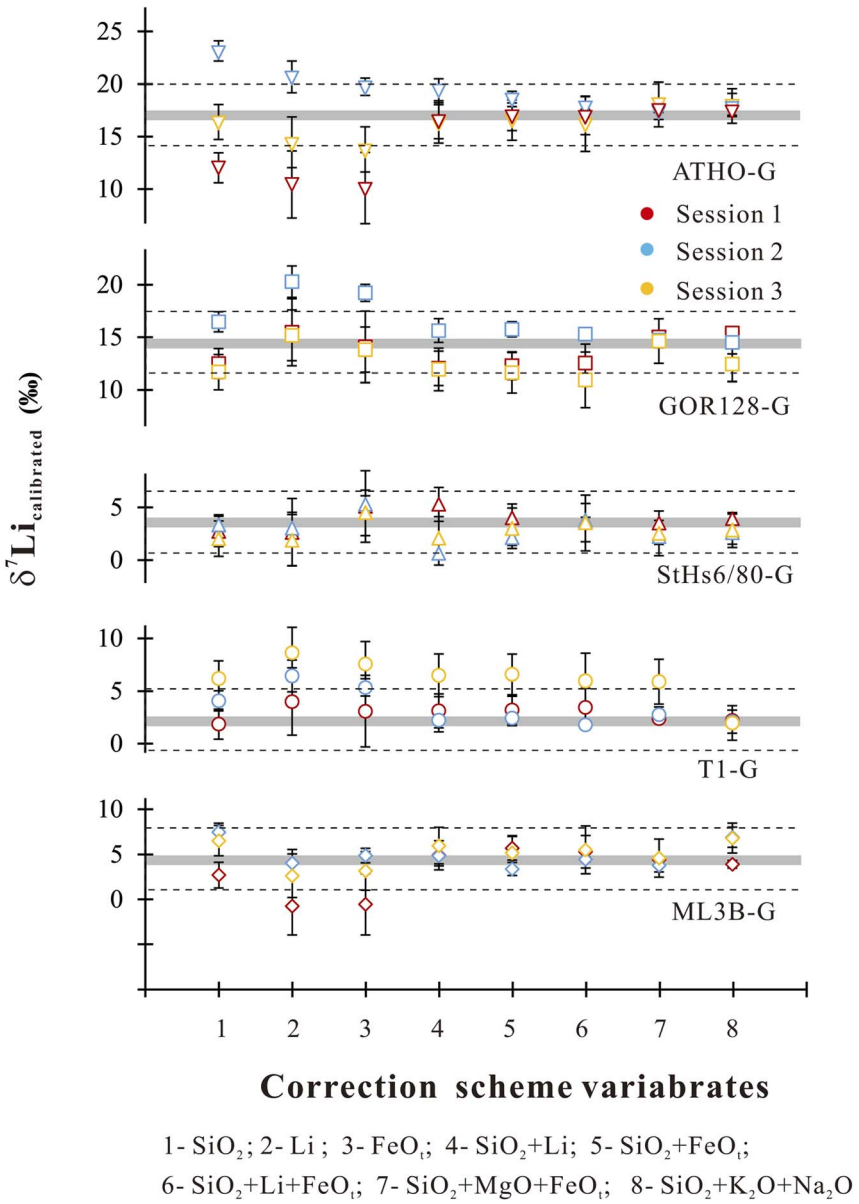

Fig. 4 δ^7Li values estimated by using different correction schemes. The grey bands represent reference values for different samples.[60] The dashed line circled the range of reproducibility within ±3 ‰ of the preferred values. The vertical bars represent the corresponding root-mean-square error for different correction schemes.

Open Access Article. Published on 30 August 2023. Downloaded on 1/27/2026 4:47:07 AM. This article is licensed under a Creative Commons Attribution-NonCommercial 3.0 Unported Licence.

by IMF and ($K_2O + Na_2O$) are more robust than considering K_2O or Na_2O alone (Fig. 3). However, the MPI-DING silicate glasses are subalkaline, making it difficult to explore the influence of alkali on the matrix effect of Li isotope analysis. It is important to keep in mind that MPI-DING silicate glasses do not cover the chemical composition of all natural glasses.

Accordingly, we used the observed correlations between IMF and a single component to establish a correction scheme. Using Origin software (2021), the IMF correction scheme could be acquired through best-fit linear regressions in the form of IMF $= d_iX_i + c$, where d_i is the empirical coefficient, X_i is the content of major and trace element i, and c is a constant. It shows robust correlations between IMF and Li, SiO_2 and FeO_t with relatively high R^2 values of >0.7 (Table 4). Under the SiO_2 correction scheme, 80% of the $\delta^7Li_{calibrated}$ values of the sample are reproduced within ±3‰ (Fig. 4) of their reference values. If using the Li content to correct IMF, 60% of the δ^7Li values are estimated to range within ±3‰ (Fig. 4). When FeO_t correction is applied, 73% of the δ^7Li values in samples are reproduced within ±3‰ (Fig. 4). It seems that, then, the SiO_2 content is most suitable to calibrate the Li isotope-IMF in silicate glasses.

4.3.2 Multivariate correction schemes. We estimated several multivariate correction schemes using the best-fit empirical equation in the form of IMF $= \sum d_iX_i + c$. Two bivariate correction schemes of SiO_2–Li and SiO_2–FeO_t, and three trivariate correction schemes of SiO_2–FeO_t–Li, SiO_2–MgO–FeO_t and SiO_2–Na_2O–K_2O are highly correlated with the variable IMF. Using SiO_2–Li, SiO_2–FeO_t and SiO_2–FeO_t–Li correction schemes, 93% of the estimated δ^7Li values are reproduced within ±3‰ of their preferred values (Fig. 4). Nearly all the δ^7Li values of samples are reproduced within ±3‰, when using SiO_2–MgO–FeO_t and SiO_2–Na_2O–K_2O correction schemes (Fig. 4). The parameters for these correction schemes are summarized in Table 5. Either way, it shows highly variable empirical coefficients d_i and constants c fitting the IMF values in different analytical sessions (Table 5). Although these correction schemes provide an improvement in the accuracy of δ^7Li compared to univariate correction schemes, there is a risk of over-defining the correction system by bringing in multiple variables.

It should be emphasized that the aforementioned multivariate correction methods cannot be implemented without taking SiO_2 into account. This indicates that the SiO_2 content has the greatest impact on the Li isotope matrix effect for silicate glasses, at least for the investigated samples. The silica-related matrix effect for silicate glasses has been previously observed to affect Li, Be, B, Mg, Ca and Al abundance,[25,29,75] and O isotope analysis.[33,37,46] The matrix effect on Li analysis has been previously noted as a function of voltage offset on low- and high-silica samples.[26,29] A mechanism for such a silica-related matrix effect may be that significant changes in Li-ion energy distribution take place as a result of the silicon-induced enhancement of ionization.[75]

Table 5 Parameters of the best-fit empirical equations for multivariate correction schemes

Analytical sessions	Parameters			
IMF = $d_{SiO_2}X_{SiO_2} + d_{Li}X_{Li} + c$	d_{SiO_2}	d_{Li}	c	R^2
Session 1	−0.82	0.19	82.14	0.91
Session 2	−0.44	−0.14	67.52	0.87
Session 3	−0.56	−0.08	65.40	0.74

Analytical sessions	Parameters			
IMF = $d_{SiO_2}X_{SiO_2} + d_{FeOt}X_{FeOt} + c$	d_{SiO_2}	d_{FeOt}	c	R^2
Session 1	−0.93	−1.01	98.91	0.94
Session 2	−0.23	1.18	44.82	0.94
Session 3	−0.49	0.59	56.21	0.81

Analytical sessions	Parameters				
IMF = $d_{SiO_2}X_{SiO_2} + d_{FeOt}X_{FeOt} + d_{Li}X_{Li} + c$	d_{SiO_2}	d_{FeOt}	d_{Li}	c	R^2
Session 1	−0.90	−1.35	−0.15	102.50	0.89
Session 2	−0.24	2.47	0.49	27.93	0.99
Session 3	−0.53	1.15	0.24	50.55	0.65

Analytical sessions	Parameters				
IMF = $d_{SiO_2}X_{SiO_2} + d_{FeOt}X_{FeOt} + d_{MgO}X_{MgO} + c$	d_{SiO_2}	d_{FeOt}	d_{MgO}	c	R^2
Session 1	−1.06	−0.97	−0.24	108.06	0.99
Session 2	−0.07	1.36	0.13	32.92	0.94
Session 3	−0.82	0.10	−0.31	81.28	0.77

Analytical sessions	Parameters				
IMF = $d_{SiO_2}X_{SiO_2} + d_{Na_2O}X_{Na_2O} + d_{K_2O}X_{K_2O} + c$	d_{SiO_2}	d_{Na_2O}	d_{K_2O}	c	R^2
Session 1	−0.97	1.88	1.66	86.66	0.99
Session 2	−0.41	−1.50	0.61	66.70	0.87
Session 3	−1.19	0.96	5.05	92.61	0.86

4.4 Online matrix effect correction

4.4.1 Online correction scheme. The observed silica-related correlations with IMF could be used as the basis of empirical corrections of the matrix effect on Li isotope analysis. Here, we develop a straightforward "online" method to correct IMF by using simultaneous detection of $^6Li^+$, $^7Li^+$ and $^{30}Si^+$ signals. The $^{30}Si^+$ signals and the IMF obtained by NanoSIMS show a solid relationship in analytical sessions. The best-fit curves are estimated by using the linear and logarithmic regressions as the form of $IMF_{corrected} = d \times {}^{30}Si^+rate + c$ and $IMF_{corrected} = d \times \ln({}^{30}Si^+rate) + c$, respectively (Fig. 5). Since the IMF is very sensitive to the instrumental conditions, the values of the empirical coefficient d and the constant c are variable in different analytical sessions (Fig. 5), suggesting that the best-fit

 This journal is © The Royal Society of Chemistry 2023

Open Access Article. Published on 30 August 2023. Downloaded on 1/27/2026 4:47:07 AM.
This article is licensed under a Creative Commons Attribution-NonCommercial 3.0 Unported Licence.

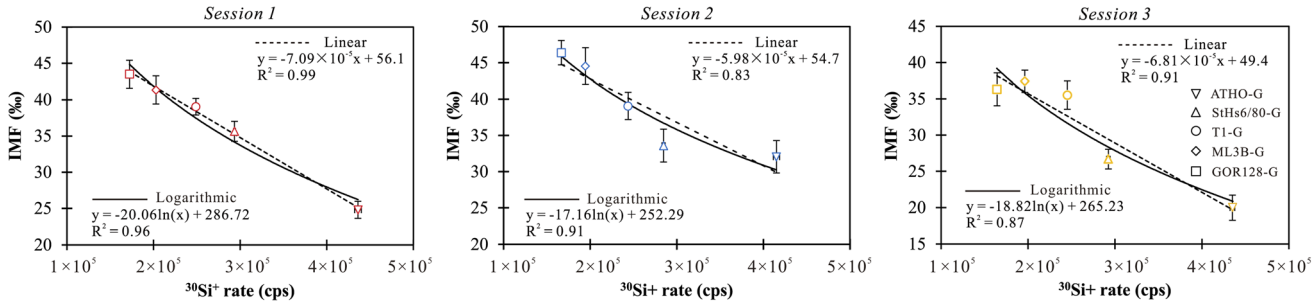

Fig. 5 IMF as a function of $^{30}Si^+$ signals. The vertical error bars are the external precision of the measurements, and the horizontal bars represent the standard deviation of the $^{30}Si^+$ counting rate in the corresponding session.

equation for Li isotopic IMF *vs.* the Si counting rate is empirical and requires continuous monitoring during analysis.

To assess the efficacy of the online-calibration strategies, four silicate glasses (*e.g.*, ATHO-G, StHs6/80-G, ML3B-G and GOR128-G) were employed to obtain the calibrated equations and to correct the IMF of T1-G, which was treated as the unknown target. The calibration proceeded using both linear and logarithmic regression equations. Using Origin software (2021), the calibrated IMF values for T1-G in each session were estimated based on the $^{30}Si^+$ signals and displayed as averages within the 95% confidence intervals (CIs). The results showed that the uncertainties of the predicted IMF range from 0.6‰–3.7‰ (1SD) for the linear regression calibration and 2.2‰–2.8‰ (1SD) for the logarithmic regression (Table 6). The accuracy of the online calibration method is estimated using the absolute difference between the IMF values measured from the analytical data and corrected using the calibration equation, denoted as $\Delta IMF = |IMF_{measured} - IMF_{corrected}|$. The results show that ΔIMF values vary from 0.7‰ to 3.5‰ in linear regression calibration and 0.4‰ to 4.4‰ in logarithmic regression (Table 6). The linear regression is slightly better than the logarithmic regression to calibrate Li isotope-IMF for silicate glasses.

4.4.2 Comparison of IMF-correction efficacy between online and offline methods. "Offline" methods to calibrate the matrix effect are commonly used, by which the quantitative determination of SiO_2 contents using EMPA in unknown samples is required to estimate IMF subsequently based on empirical correction curves.[24,25,29,33,34,76,77] Here, we compare the IMF-correction efficacy of the up-to-date "online" method with that of the conventional "offline" method.

With the aim to directly compare the accuracy of the online method with the offline method under the aforementioned analytical procedure, the first comparison is made based on the data of sessions 1–3. The efficacy of the online method has been discussed in the above section, with ATHO-G, StHs6/80-G, ML3B-G and GOR128-G employed to obtain the calibrated equations and to correct the IMF of T1-G. Using the online method, the δ^7Li of T1-G could be reproduced within 0.8–3.5‰ of its preferred value (Table 7). Then, we conduct the offline correction procedure. The best-fit curve in linear regression between the SiO_2 contents and IMF of the ATHO-G, StHs6/80-G, ML3B-G and GOR128-G is estimated to predict the IMF of T1-G. It shows that the δ^7Li of T1-G could be reproduced within 0.3–4.7‰ of the reference value (Table 7), which is equivalent to the online method.

Given that the accuracy of the online method is highly dependent on the absolute $^{30}Si^+$ intensities, it can vary considerably when the instrumental settings change. To assess the reliability of the online method, we applied different EMs for Si secondary ion detection and primary beam current individually in other independent analyses. In session 4, we used different EMs to collect Si secondary ions while maintaining other experimental conditions consistent with sessions 1–3 (Table 7). The samples ATHO-G, GOR128-G and ML3B-G were measured to calibrate the IMF of T1-G by using both online and offline methods. The results show that the δ^7Li of T1-G could be reproduced within ± 1.6‰ using the offline method (Table 7). The online method could reproduce the δ^7Li of T1-G within ± 2.2‰ of its reference values, even with a 20% reduction in the $^{30}Si^+$ intensities (Table 7).

Furthermore, we applied various primary beam intensities to analyze Li isotopes. In consideration of the effective counting rate of $^6Li^+$ ions and optimum EM capacity for $^{30}Li^+$ ions, we decreased the beam current down to 100 pA in session 5 (Table 7). Samples ATHO-G, StHs6/80-G and KL2-G were used to calibrate the IMF of T1-G. KL2-G is a basaltic MPI-DING silicate glass, which has a SiO_2 content of 50.3 ± 0.3 wt% and Li concentrations of 5.1 ± 0.5 ppm.[60] Despite a considerable shift

Table 6 The IMF and ΔIMF values corrected using linear regression and logarithmic regression for T1-G

Analytical sessions	$IMF_{corrected}$ in linear regression (‰)	Uncertainty (95% CI, ‰)	ΔIMF (‰)	$IMF_{corrected}$ in logarithmic regression (‰)	Uncertainty (95% CI, ‰)	ΔIMF (‰)
Session 1	38.3	±0.6	0.7	37.2	±2.2	1.8
Session 2	40.6	±3.7	1.6	39.5	±2.8	0.4
Session 3	32.0	±3.3	3.5	31.1	±2.8	4.4

Open Access Article. Published on 30 August 2023. Downloaded on 1/27/2026 4:47:07 AM.
This article is licensed under a Creative Commons Attribution-NonCommercial 3.0 Unported Licence.

Table 7 Comparison of "online" and "offline" methods to correct IMF and Li isotope for T1-G

Session	Primary beam current	^{7}Li yield (cps nA^{-1} ppm^{-1})	^{30}Si yield (cps nA^{-1} wt%)	IMF$_{measured}$ (‰)	Online (Si counting rate-correction)				Offline (SiO_2-correction)			
					IMF$_{corrected}$ (‰)	Uncertainty (‰)	δ^{7}Li$_{calibrated}$ (‰)	Δ^{a} (‰)	IMF$_{corrected}$ (‰)	Uncertainty (‰)	δ^{7}Li$_{calibrated}$ (‰)	Δ^{a} (‰)
1	1 nA	1244	4245	39.0	38.3	0.6	2.9	0.8	36.8	2.5	4.4	2.3
2	1 nA	1213	4158	39.1	40.6	3.7	0.6	1.5	39.5	2.7	1.8	0.3
3	1 nA	1260	4183	35.5	32.0	3.3	5.6	3.5	30.9	2.8	6.8	4.7
4	1 nA	1230	3367	8.5	10.7	0.9	0.1	2.2	10.1	0.01	0.5	1.6
5	100 pA	1110	4103	42.0	41.6	5.4	2.6	0.5	39.5	11.1	4.7	2.6

[a] $\Delta = |\delta^{7}\mathrm{Li}_{calibrated} - \delta^{7}\mathrm{Li}_{true}|$.

in the primary beam, the yield of ^{7}Li and ^{30}Si ions remained the same as those in sessions 1–3 (Table 7). In this scenario, the δ^{7}Li of T1-G could be reproduced within ± 0.5‰ by using the online method and within ± 2.6‰ by using the offline method (Table 7).

In summary, the online-calibration strategy has equivalent reproductivity to the offline method, even when there is a significant change in the Si secondary ion counts. Compared with the offline method, the online method offers time-saving advantages for analyzing Li isotopes of silicate glasses with various compositions. It is also noteworthy that our method has two drawbacks. Although MPI-DING glasses cover a wide range of compositions, from ultramafic to highly siliceous, they do not encompass all natural glasses. As a result, our method is only applicable to anhydrous subalkaline magmatic glasses that fall within the range of MPI-DING glasses. Additionally, the calibration method is entirely empirical. Therefore, further research is necessary to explore the connection between element-specific parameters and ionization models.

5. Conclusions

In this study, we conducted Li isotope analysis on MPI-DING silicate glasses by using a NanoSIMS. The secondary ions, including $^{6}Li^{+}$, $^{7}Li^{+}$ and $^{30}Si^{+}$, were detected simultaneously. The IMF exhibited variations up to 19‰ between mafic and rhyolite glasses, indicating a significant matrix effect on Li isotopic analysis in silicate glasses. Several correction models show that the IMF is strongly dependent on the chemical compositions of these silicate glasses, especially the SiO_2 contents. We found that empirical correlations between the $^{30}Si^{+}$ counting rate and IMF are useful as an IMF-correction scheme. A straightforward "online" method for the IMF calibration was then proposed taking advantage of simultaneously detected $^{6}Li^{+}$, $^{7}Li^{+}$ and $^{30}Si^{+}$ signals. By applying this calibrated strategy, the IMF and δ^{7}Li of samples can be reproduced within ±3‰ of the reference values. This method can be widely applied to anhydrous subalkaline magmatic glasses from compositional ultramafic to highly siliceous.

Author contributions

Conceptualization: R.-Y. L., J. H., W. Y., and H.-C. T. Methodology: R.-Y. L. and J. H. Investigation: R.-Y. L. and J. H. Resources: W. Y., S. H., and Y. L. Writing – original draft: R.-Y. L., and W. Y. Writing – review & editing: all authors, Supervision: W. Y. Funding acquisition: R.-Y. L., W. Y., and J. H.

Conflicts of interest

There are no conflicts to declare.

Acknowledgements

We thank Axel Schmitt and two anonymous reviewers for their constructive comments and suggestions. This study was funded

Open Access Article. Published on 30 August 2023. Downloaded on 1/27/2026 4:47:07 AM.
This article is licensed under a Creative Commons Attribution-NonCommercial 3.0 Unported Licence.

by the National Natural Science Foundation of China (No. 42103032, No. 42241103 and No. 42173036).

References

1 S. Agostini, J. G. Ryan, S. Tonarini and F. Innocenti, *Earth Planet. Sci. Lett.*, 2008, **272**, 139–147.
2 T. Elliott, A. Jeffcoate and C. Bouman, *Earth Planet. Sci. Lett.*, 2004, **220**, 231–245.
3 F. S. Genske, S. P. Turner, C. Beier, M.-F. Chu, S. Tonarini, N. J. Pearson and K. M. Haase, *Chem. Geol.*, 2014, **373**, 27–36.
4 K. Kobayashi, R. Tanaka, T. Moriguti, K. Shimizu and E. Nakamura, *Chem. Geol.*, 2004, **212**, 143–161.
5 A. G. Fairen, E. Losa-Adams, C. Gil-Lozano, L. Gago-Duport, E. R. Uceda, S. W. Squyres, J. A. Rodriguez, A. F. Davila and C. P. McKay, *Geochem., Geophys., Geosyst.*, 2015, **16**, 1172–1197.
6 S. Misra and P. N. Froelich, *Science*, 2012, **335**, 818–823.
7 P. Négrel and R. Millot, *Chem. Geol.*, 2019, **523**, 121–132.
8 F. Tong, Y. Xiao, H. Sun, Y. Wang, H. Wan, L.-F. Gou, Y. Gong, F. Huang, D.-Y. Li and Z. Hou, *Sci. Total Environ.*, 2021, 785.
9 P. A. P. von Strandmann, S. A. Kasemann and J. B. Wimpenny, *Elements: An International Magazine of Mineralogy, Geochemistry, and Petrology*, 2020, vol. 16, pp. 253–258.
10 L. A. Coogan, S. A. Kasemann and S. Chakraborty, *Earth Planet. Sci. Lett.*, 2005, **240**, 415–424.
11 K. Gallagher and T. Elliott, *Earth Planet. Sci. Lett.*, 2009, **278**, 286–296.
12 A. Jeffcoate, T. Elliott, S. Kasemann, D. Ionov, K. Cooper and R. Brooker, *Geochim. Cosmochim. Acta*, 2007, **71**, 202–218.
13 I. J. Parkinson, S. J. Hammond, R. H. James and N. W. Rogers, *Earth Planet. Sci. Lett.*, 2007, **257**, 609–621.
14 A. E. Rubin, K. M. Cooper, C. B. Till, A. J. Kent, F. Costa, M. Bose, D. Gravley, C. Deering and J. Cole, *Science*, 2017, **356**, 1154–1156.
15 A. Beinlich, T. John, J. C. Vrijmoed, M. Tominaga, T. Magna and Y. Y. Podladchikov, *Nat. Geosci.*, 2020, **13**, 307–311.
16 P. Beck, J. Barrat, M. Chaussidon, P. Gillet and M. Bohn, *Geochim. Cosmochim. Acta*, 2004, **68**, 2925–2933.
17 P. Beck, M. Chaussidon, J.-A. Barrat, P. Gillet and M. Bohn, *Geochim. Cosmochim. Acta*, 2006, **70**, 4813–4825.
18 M.-C. Liu, M. Chaussidon and N. Matsuda, *Geochim. Cosmochim. Acta*, 2023, **341**, 150–163.
19 T. Magna, U. Wiechert and A. N. Halliday, *Earth Planet. Sci. Lett.*, 2006, **243**, 336–353.
20 T. Magna, A. Deutsch, K. Mezger, R. Skála, H. M. Seitz, J. Mizera, Z. Řanda and L. Adolph, *Geochim. Cosmochim. Acta*, 2011, **75**, 2137–2158.
21 H.-M. Seitz, G. P. Brey, S. Weyer, S. Durali, U. Ott, C. Münker and K. Mezger, *Earth Planet. Sci. Lett.*, 2006, **245**, 6–18.
22 H.-M. Seitz, J. Zipfel, G. P. Brey and U. Ott, *Earth Planet. Sci. Lett.*, 2012, **329**, 51–59.
23 C. Shearer, G. Layne and J. Papike, *Geochim. Cosmochim. Acta*, 1994, **58**, 5349–5362.
24 D. R. Bell, R. L. Hervig, P. R. Buseck and S. Aulbach, *Chem. Geol.*, 2009, **258**, 5–16.
25 J. C. M. De Hoog and Edinburgh Ion Microprobe Facility, *Geostand. Geoanal. Res.*, 2018, **42**, 513–522.
26 S. A. Kasemann, A. B. Jeffcoate and T. Elliott, *Anal. Chem.*, 2005, **77**, 5251–5257.
27 T. Ludwig, H. Marschall, P. P. von Strandmann, B. Shabaga, M. Fayek and F. Hawthorne, *Mineral. Mag.*, 2011, **75**, 2485–2494.
28 M. A. Marks, R. L. Rudnick, T. Ludwig, H. Marschall, T. Zack, R. Halama, W. F. McDonough, D. Rost, T. Wenzel and E. P. Vicenzi, *Geostand. Geoanal. Res.*, 2008, **32**, 295–310.
29 L. Ottolini, P. Bottazzi and R. Vannucci, *Anal. Chem.*, 1993, **65**, 1960–1968.
30 L. Ottolini and F. C. Hawthorne, *Eur. J. Mineral.*, 1999, **11**, 679–690.
31 B. X. Su, X. Y. Gu, E. Deloule, H. F. Zhang, Q. L. Li, X. H. Li, N. Vigier, Y. J. Tang, G. Q. Tang and Y. Liu, *Geostand. Geoanal. Res.*, 2015, **39**, 357–369.
32 M. Tang, R. L. Rudnick, W. F. McDonough, M. Bose and Y. Goreva, *Earth Planet. Sci. Lett.*, 2017, **474**, 110–119.
33 E. Dubinina, A. Borisov, M. Wiedenbeck and A. Rocholl, *Chem. Geol.*, 2021, **578**, 120322.
34 J. M. Eiler, C. M. Graham and J. W. Valley, *Chem. Geol.*, 1997, **138**, 221–244.
35 J. Hao, W. Yang, Y. Luo, S. Hu, Q.-Z. Yin and Y. Lin, *J. Anal. At. Spectrom.*, 2016, **31**, 2399–2409.
36 J. Hao, S. Hu, R. Li, J. Ji, H. He, Y. Lin and W. Yang, *Atomic Spectroscopy*, 2022.
37 M. Hartley, T. Thordarson, C. Taylor and J. Fitton, *Chem. Geol.*, 2012, **334**, 312–323.
38 R. L. Hervig, P. Williams, R. M. Thomas, S. N. Schauer and I. M. Steele, *Int. J. Mass Spectrom. Ion Processes*, 1992, **120**, 45–63.
39 W. F. Hoover, S. C. Penniston-Dorland, L. P. Baumgartner, A. S. Bouvier, D. Baker, B. Dragovic and A. Gion, *Geostand. Geoanal. Res.*, 2021, **45**, 477–499.
40 S. Hu, Y. Lin, J. Zhang, J. Hao, W. Yang and L. Deng, *J. Anal. At. Spectrom.*, 2015, **30**, 967–978.
41 R.-Y. Li, J. Hao, S. Hu, W.-F. Zhang, X.-P. Xia, Y. Lin and W. Yanga, *At. Spectrosc.*, 2022, **43**, 77–83.
42 D. Vielzeuf, M. Champenois, J. W. Valley, F. Brunet and J. L. Devidal, *Chem. Geol.*, 2005, **223**, 208–226.
43 W. Yang, S. Hu, J. Zhang, J. Hao and Y. Lin, *Sci. China: Earth Sci.*, 2015, **58**, 1758–1767.
44 V. R. Deline, W. Katz, C. A. Evans Jr. and P. Williams, *Appl. Phys. Lett.*, 1978, **33**, 832–835.
45 E. H. Hauri, A. M. Shaw, J. Wang, J. E. Dixon, P. L. King and C. Mandeville, *Chem. Geol.*, 2006, **235**, 352–365.
46 R. Ickert, J. Hiess, I. Williams, P. Holden, T. Ireland, P. Lanc, N. Schram, J. Foster and S. Clement, *Chem. Geol.*, 2008, **257**, 114–128.
47 J. Zhang, Y. Lin, W. Yang, W. Shen, J. Hao, S. Hu and M. Cao, *J. Anal. At. Spectrom.*, 2014, **29**, 1934–1943.
48 J. Hao, W. Yang, W. Huang, Y. Xu, Y. Lin and H. Changela, *Surf. Interface Anal.*, 2020, **52**, 234–239.

Open Access Article. Published on 30 August 2023. Downloaded on 1/27/2026 4:47:07 AM.
This article is licensed under a Creative Commons Attribution-NonCommercial 3.0 Unported Licence.

49 J. Hao, W. Yang, S. Hu, r. Li, J. Ji, C. Hitesh and Y. Lin, *J. Anal. At. Spectrom.*, 2021, **36**, 1625–1633.
50 H. He, J. Ji, Y. Zhang, S. Hu, Y. Lin, H. Hui, J. Hao, R.-Y. Li, W. Yang, H.-C. Tian, C. Zhang, M. Anand, R. Tartese, L. Gu, J.-H. Li, D. Zhang, Q. Mao, L.-H. Jia, X.-G. Li, Y. Chen, L. Zhang, H. Ni, S. Wu, H. Wang, Q. Li, H. He, X.-H. Li and F.-Y. Wu, *Nat. Geosci.*, 2023, **16**, 294–300.
51 P. Hoppe, S. Cohen and A. Meibom, *Geostand. Geoanal. Res.*, 2013, **37**, 111–154.
52 S. Hu, Y. Lin, W. Yang, W.-R. Z. Wang, J. Zhang, J. Hao and W. Xing, *Sci. China: Earth Sci.*, 2016, **59**, 2155–2164.
53 S. Hu, H. He, J. Ji, Y. Lin, H. Hui, M. Anand, R. Tartèse, Y. Yan, J. Hao, R. Li, L. Gu, Q. Guo, H. He and Z. Ouyang, *Nature*, 2021, **600**, 49–53.
54 J. Ji, H. He, S. Hu, Y. Lin, H. Hui, J. Hao, R. Li, W. Yang, Y. Yan, H. Tian, C. Zhang, M. Anand, R. Tartèse, L. Gu, J. Li, D. Zhang, Q. Mao, L. Jia, Y. Chen, S. Wu, H. Wang, H. He, X. Li and F. Wu, *Earth Planet. Sci. Lett.*, 2022, **591**, 117636.
55 W. Yang, Y.-T. Lin, J.-C. Zhang, J.-L. Hao, W.-J. Shen and S. Hu, *J. Anal. At. Spectrom.*, 2012, **27**, 479–487.
56 W. Yang, Y. Lin, J. Hao, J. Zhang, S. Hu and H. Ni, *Contrib. Mineral. Petrol.*, 2016, **171**, 28.
57 J. Zhang, Y. Lin, W. Yang, J. Hao and S. Hu, *Int. J. Mass Spectrom.*, 2016, **406**, 48–54.
58 J. Zhang, Y. Lin, J. Yan, J. Li and W. Yang, *Anal. Methods*, 2017, **9**, 6653–6661.
59 K. P. Jochum, D. B. Dingwell, A. Rocholl, B. Stoll, A. W. Hofmann, S. Becker, A. Besmehn, D. Bessette, H.-J. Dietze, P. Dulski, J. Erzinger, E. Hellebrand, P. Hoppe, I. Horn, K. Janssens, G. A. Jenner, M. Klein, W. F. McDonough, M. Maetz, K. Mezger, C. Müker, I. K. Nikogosian, C. Pickhardt, I. Raczek, D. Rhede, H. M. Seufert, S. G. Simakin, A. V. Sobolev, B. Spettel, S. Straub, L. Vincze, A. Wallianos, G. Weckwerth, S. Weyer, D. Wolf and M. Zimmer, *Geostand. Newsl.*, 2000, **24**, 87–133.
60 K. P. Jochum, B. Stoll, K. Herwig, M. Willbold, A. W. Hofmann, M. Amini, S. Aarburg, W. Abouchami, E. Hellebrand and B. Mocek, *Geochem., Geophys., Geosyst.*, 2006, **7**, 1–44.
61 S. Seetharaman, *Treatise on Process Metallurgy Volume 1: Process Fundamentals*, Newnes, 2013.
62 J. Cabato, R. Altherr, T. Ludwig and H.-P. Meyer, *Contrib. Mineral. Petrol.*, 2013, **165**, 1135–1154.
63 S. Decitre, E. Deloule, L. Reisberg, R. James, P. Agrinier and C. Mével, *Geochem., Geophys., Geosyst.*, 2002, **3**, 1–20.
64 Y. Y. Gao, X. H. Li, W. L. Griffin, Y. J. Tang, N. J. Pearson, Y. Liu, M. F. Chu, Q. L. Li, G. Q. Tang and S. Y. O'Reilly, *Sci. Rep.*, 2015, **5**, 16878.
65 P. J. le Roux, *J. Anal. At. Spectrom.*, 2010, **25**, 1033–1038.
66 X.-H. Li, Q.-L. Li, Y. Liu and G.-Q. Tang, *J. Anal. At. Spectrom.*, 2011, **26**, 352–358.
67 J. Lin, Y. Liu, Z. Hu, W. Chen, L. Zhang and H. Chen, *Geostand. Geoanal. Res.*, 2019, **43**, 277–289.
68 L. Nasdala, F. Corfu, J. W. Valley, M. J. Spicuzza, F. Y. Wu, Q. L. Li, Y. H. Yang, C. Fisher, C. Münker and A. K. Kennedy, *Geostand. Geoanal. Res.*, 2016, **40**, 457–475.
69 F. Richter, M. Chaussidon, E. B. Watson, R. Mendybaev and V. Homolova, *Geochim. Cosmochim. Acta*, 2017, **219**, 124–142.
70 L. K. Steinmann, M. Oeser, I. Horn, H.-M. Seitz and S. Weyer, *J. Anal. At. Spectrom.*, 2019, **34**, 1447–1458.
71 K. Baral, A. Li and W. Y. Ching, *J. Phys. Chem. A*, 2017, **121**, 7697–7708.
72 O. Gedeon, J. Zemek and K. Jurek, *J. Non-Cryst. Solids*, 2008, **354**, 1169–1171.
73 C. McLaren, W. Heffner, R. Tessarollo, R. Raj and H. Jain, *Appl. Phys. Lett.*, 2015, **107**, 184101.
74 Y. H. Rim, M. Kim, C. G. Baek and Y. S. Yang, *J. Alloys Compd.*, 2020, 827.
75 N. Shimizu, *Int. J. Mass Spectrom. Ion Processes*, 1986, **69**, 325–338.
76 L.-G. Wu, Q.-L. Li, Y. Liu, G.-Q. Tang, K. Lu, X.-X. Ling and X.-H. Li, *J. Anal. At. Spectrom.*, 2020, **35**, 1607–1613.
77 J. Y. Xu, Q. L. Li, G. Q. Tang, K. Lu, Y. Liu, L. J. Feng and J. C. Melgarejo, *Anal. Chem.*, 2022, **94**, 7944–7951.

 This journal is © The Royal Society of Chemistry 2023